Inverse Ising inference with correlated samples

Benedikt Obermayer[1,2] and Erel Levine[1]

[1] Department of Physics and Center for Systems Biology, Harvard University, Cambridge MA 02138, USA
[2] Max-Delbrück-Center for Molecular Medicine, Berlin-Buch, Germany
E-mail: benedikt.obermayer@mdc-berlin.de and elevine@fas.harvard.edu

Abstract

Correlations between two variables of a high-dimensional system can be indicative of an underlying interaction, but can also result from indirect effects. Inverse Ising inference is a method to distinguish one from the other. Essentially, the parameters of the least constrained statistical model are learned from the observed correlations such that direct interactions can be separated from indirect correlations. Among many other applications, this approach has been helpful for protein structure prediction, because residues which interact in the 3D structure often show correlated substitutions in a multiple sequence alignment. In this context, samples used for inference are not independent but share an evolutionary history on a phylogenetic tree. Here, we discuss the effects of correlations between samples on global inference. Such correlations could arise due to phylogeny but also via other slow dynamical processes. We present a simple analytical model to address the resulting inference biases, and develop an exact method accounting for background correlations in alignment data by combining phylogenetic modeling with an adaptive cluster expansion algorithm. We find that popular reweighting schemes are only marginally effective at removing phylogenetic bias, suggest a rescaling strategy that yields better results, and provide evidence that our conclusions carry over to the frequently used mean-field approach to the inverse Ising problem.

Keywords: inverse problems, statistical sequence analysis, phylogenetic inference
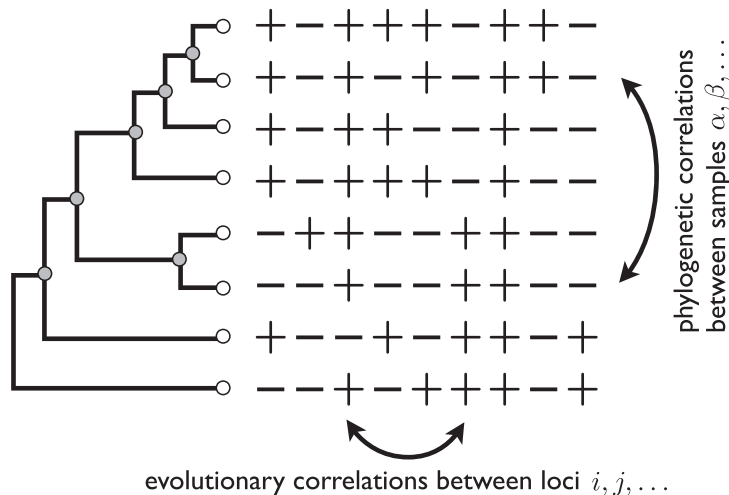
Figure 1. Data are given in the form of an alignment **X** of N loci across M samples on a phylogenetic tree with M external nodes (white). Data are unknown for $M - 2$ ancestral nodes (gray), which are therefore integrated out. Inference of interactions between loci from observable evolutionary correlations is confounded by phylogenetic correlations between samples.

An exciting confluence of techniques from statistical physics, computer science and information theory over the last decade has yielded new methods for the study of high-dimensional interacting systems, including neuronal networks [1], bird flocks [2], justices on the US supreme court [3], gene expression networks [4], protein–protein interactions [5], transcription factor binding motifs [6], HIV vaccine design [7], and protein folding [8–12]. Briefly, a maximum-entropy formalism [13, 14] is used to infer the parameters of a Boltzmann-like probability distribution such that its first two moments coincide with the ones observed in the data. These parameters in turn can be used to distinguish direct interactions from indirect correlations. In the comparative genomics field, which is boosted by the rapid growth of sequenced genomes, such methods are used to study evolutionary correlations in protein sequences, fueled by the observation that sequence changes at one locus are frequently accompanied by compensatory changes at another locus. Assuming that this type of evolutionary constraint results from a physical interaction of the involved residues, inference of such direct correlations in multiple alignments of homologous protein sequences allows one to identify pairs of protein residues in close spatial proximity within the tertiary structure, as opposed to indirect correlations due to intermediaries [15]. This can be used to aid and greatly simplify computational protein structure prediction [8–11].

Consider an alignment **X** of binary sequences from M samples (e.g., species, numbered by greek indices) for N sites (e.g., genomic loci, numbered by roman indices), see figure 1. In a comparative genomics application, the two states $X_{\alpha i} = \pm 1$ could signify whether or not the sequence agrees with a consensus sequence, usage of a preferred or a rare codon, the presence or absence of a binding site, or any other binary observation. To obtain a description of these data with minimal prior assumptions means to infer parameters **h** and **J** of the maximum-entropy probability distribution $P(\mathbf{x}) = Z^{-1} \exp\left(\sum_i h_i x_i + \sum_{i<j} J_{ij} x_i x_j \right)$ that reproduces the observed moments $m_i = \sum_\alpha X_{\alpha i}/M$ and $m_{ij} = \sum_\alpha X_{\alpha i} X_{\alpha j}/M$. This is known as 'inverse Ising'

inference, and a complex global problem, since in general all inferred parameters are interdependent.

Algorithms proposed so far include small-correlation expansions [2, 16], mean-field methods [17–19], belief propagation [5, 20], a cluster expansion method [21, 22] and logistic regression [23, 24]. A common assumption is that the samples $\mathbf{X}_\alpha$ are independent of each other. This, however, is often not the case: for instance, aligned homologous sequences share a common evolutionary history, represented by a phylogenetic tree. Generally, the resulting correlations are always positive and give rise to biases that do not average out within the sample but lead to coherent fluctuations. Since the underlying evolutionary experiment normally cannot be repeated, there is no way to obtain a less biased estimate from independent replicates. Moreover, available sequences are usually not a fair sample of the evolutionary history, because some clades have received more attention or were more thoroughly sequenced than others (for instance, primates within mammals, or mammals within vertebrates). Alternatively, positive correlations between samples could arise when sampling too densely from a time series or Markov chain. Disregarding such correlations between samples can therefore lead to over-estimation of true correlations between sites, and significantly bias inferred parameters of the corresponding model.

Previously it has been suggested that one could account for the redundancy in the data, e.g., due to oversampling of closely related species, by weighting the samples when calculating moments, $\tilde{m}_i = \sum_\alpha w_\alpha X_{\alpha i}$ [5, 8, 9, 25]. The weights w_α are chosen by heuristic methods, among them specialized weighting schemes for data from a phylogenetic tree [26, 27]. However, this approach may lead to loss of information, and cannot correct for global biases. Alternatively, it was proposed that the coherent nature of phylogenetic correlations leads to a pronounced signal primarily in the first eigenvector of the observed correlations matrix [28, 29] and can thus be efficiently removed. Other studies (reviewed in [30]) compared observed evolutionary correlations against a background expected from the phylogeny, or obtained estimates within an explicit phylogenetic model, but have not addressed the full inverse problem.

Here, we analyze inference biases due to correlated samples and propose an inverse Ising inference method to account for such correlations. Our approach is motivated by the special case of phylogenetic correlations, but our methods and conclusions also apply to between-sample correlations arising from slow dynamical processes in other contexts unrelated to biology. The paper is organized as follows: section 1 contains a definition of the problem and a detailed description of analytical and numerical methods used. The latter are not essential for a first reading of section 2, which contains a discussion of our main results. Section 3 discusses potential applications of our findings in the context of protein structure prediction.

1. Methods

1.1. Definition of the problem

Although evolutionary dynamics does not generally occur in equilibrium, observable correlations between samples can often be well approximated by an equilibrium process. We thus assume that the entire dataset is one representative sample generated by such a known process, and estimate the remaining parameters causing deviations from expectation by maximum likelihood. Specifically, our unified framework minimizes the cross-entropy

$$S = -\frac{1}{M} \ln \mathcal{P}(\mathbf{X} \mid \mathbf{h}, \mathbf{J}) \tag{1}$$

of the entire alignment with respect to the unknown parameter sets $\mathbf{h}$ and $\mathbf{J}$, where the fields $\mathbf{h}$ cause deviations of single loci from the background and the couplings $\mathbf{J}$ connect pairs of loci. This minimization is equivalent to maximizing the log-likelihood of the model given (all) the data. The M species represent the leaves of an (unrooted) phylogenetic tree, with additional $M - 2$ hidden (or ancestral) nodes in the interior of the tree for unknown states of common ancestors (figure 1). Including these nodes into our calculation gives a larger data matrix $\mathbf{X}'$. Marginalizing over unobserved ancestral states, the probability of the data under the model reads

$$\mathcal{P}(\mathbf{X} \mid \mathbf{h}, \mathbf{J}) = \frac{1}{\mathcal{Z}} \mathrm{Tr}' e^{-\mathcal{H}(\mathbf{X}')}. \tag{2}$$

Here, we set the energy unit $k_{\mathrm{B}}T = 1$, Tr' denotes a partial trace over the ancestral nodes only (i.e., the gray nodes in figure 1), $\mathcal{Z} = \mathrm{Tr}\, e^{-\mathcal{H}}$ is the partition function with the trace performed over all nodes, and the Hamiltonian $\mathcal{H}$ for a configuration $\mathbf{x} = (x_{\alpha i})$ is given by

$$\mathcal{H}(\mathbf{x}) = \sum_i \mathcal{H}_0\left(\mathbf{x}_i^T\right) - \sum_{\alpha,i} h_i x_{\alpha i} - \sum_{\alpha, i < j} J_{ij} x_{\alpha i} x_{\alpha j}. \tag{3}$$

Different from a standard phylogenetic approach, we model the dependencies induced by shared evolutionary history using a 'phylogenetic' Hamiltonian

$$\mathcal{H}_0(\mathbf{x}) = -\sum_\alpha g_\alpha x_\alpha - \sum_{\alpha < \beta} K_{\alpha\beta} x_\alpha x_\beta \tag{4}$$

with fields and couplings $\mathbf{g}$ and $\mathbf{K}$, respectively, where $K_{\alpha\beta}$ is nonzero only for neighbors on the phylogenetic tree, decreasing roughly with the logarithm of inverse branch length [31]. The fields g_α serve to prescribe a prior distribution on the states (e.g., beliefs about missing data or other biases for some species). By means of a reference 'background' data set $\mathbf{X}^{(0)}$, the parameters of this model (M fields at the leaves of the tree and $2M - 3$ couplings) can be inferred by matching the first two moments $\mu_\alpha = \langle X_\alpha^{(0)} \rangle$ and $\mu_{\alpha\beta} = \langle X_\alpha^{(0)} X_\beta^{(0)} \rangle$ between observed values and those calculated from $\mathcal{H}_0$ (see section 1.3.3 below). We note that this choice of phylogenetic model is based on comparable assumptions as more standard phylogenetic Markov models, and the differences lie mostly in how their parameters are interpreted (see discussion for details).

1.2. A simple linear problem and local inference

We consider first a simplified version of the problem, where the correlation structure between the M species follows a linear chain rather than a tree. This model does not have hidden ancestral nodes and amounts to N coupled Ising chains with fields $\mathbf{h}$, between-loci couplings $\mathbf{J}$ and between-sample coupling $K_{\alpha\beta} = K_0 \delta_{\alpha, \beta-1}$ (i.e., between neighboring rows in figure 1). In this case, the partition function can be calculated using textbook transfer matrix methods. We will further restrict ourselves to the simplest case $N = 2$.

Specifically, we use a system of $N = 2$ Ising chains with fields h_1 and h_2, intra-chain coupling K and inter-chain coupling J_{12}. For large M, the partition function reads

$$\frac{1}{M} \ln \mathcal{Z}\left(h_1, h_2, J_{12}, K\right) = \ln\left[\cosh^2 K \cosh J_{12} \cosh h_1 \cosh h_2 \right] + \ln \Lambda + \mathcal{O}\left(M^{-1}\right). \qquad (5)$$

Here, Λ is the largest eigenvalue of the transfer matrix, which can be written as

$$\text{diag}\left(1 + T, 1 - T, 1 - T, 1 + T\right)$$

$$\times \left\{ \begin{bmatrix} (1 + U_1)(1 + R) & (1 + U_1)(1 - R) \\ (1 - U_1)(1 - R) & (1 - U_1)(1 + R) \end{bmatrix} \otimes \begin{bmatrix} (1 + U_2)(1 + R) & (1 + U_2)(1 - R) \\ (1 - U_2)(1 - R) & (1 - U_2)(1 + R) \end{bmatrix} \right\}, \qquad (6)$$

using $R = \tanh K$, $T = \tanh J_{12}$, and $U_{1/2} = \tanh h_{1/2}$, respectively. The eigenvalue is computed by solving

$$256 R^4 \left(T^2 - 1\right)^2 \left(U_1^2 - 1\right)^2 \left(U_2^2 - 1\right)^2$$

$$- 64 R^2 (R + 1)^2 \left(T^2 - 1\right)\left(U_1^2 - 1\right)\left(U_2^2 - 1\right)(TU_1U_2 - 1)\Lambda$$

$$+ 16 R\left[R^2 \left(U_1^2 \left(T^2\left(2U_2^2 - 1\right) - 1\right) - \left(T^2 + 1\right)U_2^2 + 2\right)\right.$$

$$+ 2R\left(T^2 - 1\right)\left(U_1^2 U_2^2 - 1\right) + U_1^2\left(T^2\left(2U_2^2 - 1\right) - 1\right) - \left.\left(T^2 + 1\right)U_2^2 + 2\right]\Lambda^2$$

$$- 4(R + 1)^2 (TU_1U_2 + 1)\Lambda^3 + \Lambda^4 = 0. \qquad (7)$$

1.2.1. Numerical solution. Numerical estimates $\hat{h}_{1/2}$ and $\hat{J}_{12}$ for the fields and the coupling, respectively, are calculated from the measured moments $m_1 = \frac{1}{M}\sum_\alpha X_{\alpha,1}$, $m_2 = \frac{1}{M}\sum_\alpha X_{\alpha,2}$ and $m_{12} = \frac{1}{M}\sum_\alpha X_{\alpha,1} X_{\alpha,2}$ by minimizing the entropy:

$$\mathcal{S}\left(\hat{h}_1, \hat{h}_2, \hat{J}_{12}\right) = -\hat{h}_1 m_1 - \hat{h}_2 m_2 - \hat{J}_{12} m_{12} + \frac{1}{M} \ln \mathcal{Z}\left(\hat{h}_1, \hat{h}_2, \hat{J}_{12}, K\right)$$

$$+ \mu_2\left(\hat{h}_1^2 + \hat{h}_2^2\right) + \gamma_2 \hat{J}_{12}^2 + C, \qquad (8)$$

where the second line includes two regularization terms and a constant $C = \frac{1}{M}\sum_i \mathcal{H}_0(\mathbf{X}_i) = -\frac{K}{M}\sum_\alpha (X_{\alpha,1}X_{\alpha+1,1} + X_{\alpha,2}X_{\alpha+1,2})$ that is ignored, such that only the partition function $\mathcal{Z}$ retains a K-dependence.

1.2.2. Analytical solution. In principle, we could use the above expression for the partition function and compute the expected values $\langle m_i \rangle = \frac{\partial \ln \mathcal{Z}}{M \partial h_i}$ and $\langle m_{ij} \rangle = \frac{\partial \ln \mathcal{Z}}{M \partial J_{ij}}$ for $i, j = 1, 2$. Assuming that measured sample averages m_i and m_{ij} are representative and can be used to approximate $\langle m_i \rangle$ and $\langle m_{ij} \rangle$, respectively, these equations would then be solved to get $\hat{h}_i$ and $\hat{J}_{ij}$ with an estimated background coupling $K = \hat{K}$. Due to the quartic root in equation (7) this is analytically impractical, even in the simple case $N = 2$. We therefore treat fields and couplings independently. While it is possible (but tedious) to expand $\mathcal{Z}$ in h_i and J_{ij}, it is much simpler to get the leading order results by solving the associated simple systems instead.

Inferring a field. To first order we ignore the coupling J_{ij}, and only deal with one single chain of length M, with intra-chain coupling $K = \text{atanh } R$ and field $h_i = \text{atanh } U_i$. The partition

function is

$$\frac{1}{M} \ln \mathcal{Z} = \ln \frac{1 + R + \sqrt{(1 - R)^2 + 4\,RU_i^2}}{\sqrt{1 - R^2}\,\sqrt{1 - U_i^2}}. \tag{9}$$

From this, we compute the average magnetization as

$$\langle m_i \rangle = \frac{\partial \ln \mathcal{Z}}{M \partial h_i} = \frac{(1 + R)U_i}{\sqrt{(1 - R)^2 + 4\,RU_i^2}} = \frac{1 + R}{1 - R} h_i + \mathcal{O}\left(h_i^3\right), \tag{10}$$

meaning that the inferred fields $\hat{h}_i$ can be calculated from observed magnetizations m_i as in equation (24a) below with $U_i = \tanh \hat{h}_i$. For small fields (and hence small magnetization), this corresponds to the expression

$$\hat{h}_i = \frac{1 - \hat{R}}{1 + \hat{R}} m_i + \mathcal{O}\left(m_i^3\right). \tag{11}$$

Inferring a coupling. Here, we consider two coupled chains with intra-chain coupling $K = \operatorname{atanh} R$ and inter-chain coupling $J_{ij} = \operatorname{atanh} T_{ij}$, but no field. The partition function for this case is given by

$$\frac{1}{M} \ln \mathcal{Z} = \ln \frac{2\left[1 + R^2 + \sqrt{\left(1 - R^2\right)^2 + 4T_{ij}^2 R^2}\right]}{\left(1 - R^2\right)\sqrt{1 - T_{ij}^2}}. \tag{12}$$

This produces an average pair magnetization

$$\langle m_{ij} \rangle = \frac{\partial \ln \mathcal{Z}}{M \partial J_{ij}} = \frac{\left(1 + R^2\right)T_{ij}}{\sqrt{\left(1 - R^2\right)^2 + 4R^2 T_{ij}^2}} = \frac{1 + R^2}{1 - R^2} J_{ij} + \mathcal{O}\left(J_{ij}^3\right), \tag{13}$$

meaning that the coupling J_{ij} is derived from observed moments m_{ij} as in equation (24b) below. For small J_{ij}, we can approximate

$$\hat{J}_{ij} = \frac{1 - \hat{R}^2}{1 + \hat{R}^2} m_{ij} + \mathcal{O}\left(m_{ij}^3\right). \tag{14}$$

Again, ignoring the correlations between samples ($\hat{K} = 0$) gives higher $\hat{J}_{ij}$ than when using a finite value.

Inference errors. Since the intra-chain correlations introduce coherent fluctuations, the sample averages m_i and m_{ij} can be quite different from the thermodynamic averages $\langle m_i \rangle = \frac{\partial \ln \mathcal{Z}}{M \partial h_i}$ and $\langle m_{ij} \rangle = \frac{\partial \ln \mathcal{Z}}{M \partial J_{ij}}$, respectively. We can quantify the leading-order contributions to the expected inference errors $\Delta \hat{h}_i^2 = \langle (\hat{h}_i - h_i)^2 \rangle$ and $\Delta \hat{J}_{ij}^2 = \langle (\hat{J}_{ij} - J_{ij})^2 \rangle$, by expanding in the expected fluctuations.

The expected error $\Delta h_i^2 = \langle (\hat{h}_i(m_i) - h_i)^2 \rangle$ when using the observed value m_i for inference is estimated by expanding in the difference between the error for an average observation $\langle m_i \rangle$

and the average error:

$$\left\langle \left(\hat{h}_i(m_i) - h_i \right)^2 \right\rangle = \left(\hat{h}_i\left(\langle m_i \rangle \right) - h_i \right)^2 + \left[\left\langle \left(\hat{h}_i(m_i) - h_i \right)^2 \right\rangle - \left(\hat{h}_i\left(\langle m_i \rangle \right) - h_i \right)^2 \right]$$

$$\approx \left(\hat{h}_i\left(\langle m_i \rangle \right) - h_i \right)^2 + \frac{\partial \left(\hat{h}_i\left(\langle m_i \rangle \right) - h_i \right)^2}{2\partial \langle m_i \rangle^2} \left[\langle m_i^2 \rangle - \langle m_i \rangle^2 \right], \qquad (15)$$

where from equation (9) we get

$$\langle m_i^2 \rangle - \langle m_i \rangle^2 = \frac{\partial \ln \mathcal{Z}}{M^2 \partial h_i^2} = \frac{1 + R}{M(1 - R)} - \frac{(1 + R)(1 + R(4 + R))}{M(1 - R)^3} h_i^2 + \mathcal{O}\left(h_i^4 \right). \qquad (16)$$

Note that the inferred field $\hat{h}_i$ of equation (11) uses the *assumed* intra-chain coupling $\hat{K}$, while the average magnetization $\langle m_i \rangle$ from equation (10) and the fluctuation corrections $\langle m_i^2 \rangle - \langle m_i \rangle^2$ from equation (16) are calculated with the *actual* intra-chain coupling K_0 (via $R = \tanh K_0$). Combining these results in equation (15) gives equation (25a) below.

The expected error $\langle (\hat{J}_{ij} - J_{ij})^2 \rangle$ in the coupling is then similarly estimated by writing

$$\left\langle \left(\hat{J}_{ij}(m_{ij}) - J_{ij} \right)^2 \right\rangle = \left(\hat{J}_{ij}\left(\langle m_{ij} \rangle \right) - J_{ij} \right)^2$$

$$+ \left[\left\langle \left(\hat{J}_{ij}(m_{ij}) - J_{ij} \right)^2 \right\rangle - \left(\hat{J}_{ij}\left(\langle m_{ij} \rangle \right) - J_{ij} \right)^2 \right]$$

$$\approx \left(\hat{J}_{ij}\left(\langle m_{ij} \rangle \right) - J_{ij} \right)^2 + \frac{\partial \left(\hat{J}_{ij}\left(\langle m_{ij} \rangle \right) - J_{ij} \right)^2}{2\partial \langle J_{ij} \rangle^2} \left[\langle m_{ij}^2 \rangle - \langle m_{ij} \rangle^2 \right]. \qquad (17)$$

We use equation (12) to get

$$\langle m_{ij}^2 \rangle - \langle m_{ij} \rangle^2 = \frac{\partial \ln \mathcal{Z}}{M^2 \partial J_{ij}^2} = \frac{1 + R^2}{M\left(1 - R^2\right)} - \frac{\left(1 + R^2\right)\left(1 + R^2\left(4 + R^2\right)\right)}{M\left(1 - R^2\right)^3} J_{ij}^2 + \mathcal{O}\left(J_{ij}^4 \right). \quad (18)$$

Using equations (13) and (18) with $R = \tanh K_0$ in equation (17), and equation (14) with $\hat{R} = \tanh \hat{K}$ gives equation (25b) below.

1.3. Numerical approach for global inference and correlations with a tree structure

In general, one is interested in inferring all fields and couplings simultaneously. At the same time, the correlation structure between samples is often heterogeneous. In particular, in comparative genomics applications some samples are often more similar to each other than others, reflecting the degree of shared ancestry summarized in a phylogenetic tree. Below, we detail a numerical procedure to perform global inference in the presence of between-sample correlations with a tree structure. The basic idea is to break up the system into small clusters of n sites [21] and then to condense all n values from one sample for each cluster into a single 2^n-dimensional Potts spin. The interaction graph between these variables has a tree topology, and the partition function can be calculated in linear time [20]. Note that although the linear

chain discussed before can be seen as a special case of the tree topology (and indeed the transfer matrix recursions are related to the belief propagation approach used below), it is much harder to derive analytical results for a tree, even when between-sample couplings are all identical: fixed points of transfer matrix or belief propagation recursions apply to *bulk* spins, while observations with phylogenetic correlations come from the *leaves* of the tree, and thus represent *surface states* of the system.

In the following, we show how to evaluate equation (2) using belief propagation where it is implicitly assumed that N is a small number. The next subsection recapitulates the cluster expansion algorithm from [21, 22] that can be used to systematically break down a large system into a collection of small interacting clusters.

1.3.1. Evaluation of equation (2).   We write $\ln \mathcal{P}(\mathbf{X}|\mathbf{h}, \mathbf{J}) = \ln \mathcal{Z}' - \ln \mathcal{Z}$, where the restricted partition function $\mathcal{Z}'$ is computed by performing the trace only over hidden ancestral nodes, with leaf nodes fixed to observed values. We compute these two partition functions from the Bethe free energy using the same procedure [20]. In general, the Bethe free energy reads

$$\ln \mathcal{Z} = -\sum_{(\alpha,\beta)} \sum_{\mathbf{x}_\alpha,\mathbf{x}_\beta} P_2\left(H_\alpha^h + H_\beta^h + H_{\alpha\beta}^J + \ln P_2\right) + \sum_\alpha (|\partial\alpha| - 1) \sum_{\mathbf{x}_\alpha} P_1\left(H_\alpha^h + \ln P_1\right). \tag{19}$$

Here, we introduced marginal distributions $P_2(\mathbf{x}_\alpha, \mathbf{x}_\beta)$ and $P_1(\mathbf{x}_\alpha)$, and re-organized terms of the Hamiltonian as follows: $H_\alpha^h = -\sum_i (\hat{g}_\alpha + h_i) x_{\alpha i} - \sum_{i<j} J_{ij} x_{\alpha i} x_{\alpha j}$ comes from the effective Potts field for node α and $H_{\alpha\beta}^J = -\sum_i \hat{K}_{\alpha\beta} x_{\alpha i} x_{\beta i}$ stems from the Potts coupling between two nodes. The first term in equation (19) sums over values of neighboring nodes (α, β) and the second term runs over single nodes α weighted by the number $|\partial\alpha|$ of neighbors. The marginal distribution $P_1(\mathbf{x}_\alpha)$ of a single Potts variable $\mathbf{x}_\alpha$ at node α is given by:

$$P_1(\mathbf{x}_\alpha) \simeq e^{-H_\alpha^h} \prod_{\beta \in \partial\alpha} \sum_{\mathbf{x}_\beta} e^{-H_{\alpha\beta}^J} P_{\beta\to\alpha}(\mathbf{x}_\beta), \tag{20}$$

where $\simeq$ means equality up to normalization ($\sum_{\mathbf{x}_\alpha} P_1(\mathbf{x}_\alpha) = 1$) and the product includes all neighbors $\partial\alpha$ of node α. The distribution $P_2(\mathbf{x}_\alpha, \mathbf{x}_\beta)$ for a pair of neighboring nodes reads

$$P_2(\mathbf{x}_\alpha, \mathbf{x}_\beta) \simeq P_{\alpha\to\beta}(\mathbf{x}_\alpha) e^{-H_{\alpha\beta}^J} P_{\beta\to\alpha}(\mathbf{x}_\beta). \tag{21}$$

Finally, both distributions use messages or beliefs $P_{\alpha\to\beta}(\mathbf{x}_\alpha)$, which are computed from the recursion

$$P_{\alpha\to\beta}(\mathbf{x}_\alpha) \simeq e^{-H_\alpha^h} \prod_{\gamma \in \partial\alpha\setminus\beta} \sum_{\mathbf{x}_\gamma} e^{-H_{\alpha\gamma}^J} P_{\gamma\to\alpha}(\mathbf{x}_\gamma). \tag{22}$$

These equations are evaluated along the tree, in one pass from the ancestral nodes outwards to the leaves, in a second pass from the leaves inwards. For the restricted partition function $\mathcal{Z}'$, we use the same method, where messages for a leaf α are simply fixed at the observed value $\mathbf{X}_\alpha$ by setting $P_{\alpha\to\beta}(\mathbf{x}_\alpha) = \delta(\mathbf{x}_\alpha, \mathbf{X}_\alpha)$. The entropy $S = -\frac{1}{M}[\ln \mathcal{Z}' - \ln \mathcal{Z}]$ is then minimized with respect to the $N(N+1)/2$ parameters $\mathbf{h}$ and $\mathbf{J}$ by numerical optimization [32], adding L_2-regularization terms as prior on the coefficients. Our approach can readily be adopted to the case where only (a small number of) nonzero entries in J_{ij} are to be inferred:

adding L_1-regularization terms $\gamma_1 \| \mathbf{J} \|_1$ and using appropriate optimization methods instead enforces sparsity of the inferred matrix $\hat{\mathbf{J}}$ [24, 33, 34].

1.3.2. Cluster expansion for larger systems.   We expand the entropy S in contributions from successively larger clusters [21, 22],

$$S = S_0 + \sum_i \Delta S_i + \sum_{i,j} \Delta S_{ij} + \dots . \tag{23}$$

A cluster $C = (i_1 \dots i_n)$ of n spins is only included if its contribution $\Delta S_C = S_C - S_{0,C} - \sum_{i \in C} \Delta S_i - \sum_{i,j \in C} \Delta S_{ij} - \dots$ exceeds in absolute value a predefined threshold Θ after the contributions of all subclusters have been removed. Here, the entropy $S_C = -\frac{1}{M} \ln \mathcal{P}_C (\mathbf{X}_C^T | \mathbf{h}, \mathbf{J}) = -\frac{1}{M} [\ln \mathcal{Z}_C{}' - \ln \mathcal{Z}_C]$ is computed from the difference in Bethe free energy equation (19). Larger clusters are recursively tested by merging smaller overlapping clusters. Each cluster's entropy is separately minimized with respect to its $n(n + 1)/2$ associated parameters $\mathbf{h}$ and $\mathbf{J}$, and optimal parameters from overlapping clusters are summed up as described in [21, 22]. The procedure terminates when no larger cluster with significant contribution to the entropy can be found. Finally, while a mean-field approximation as in [21] could be used as well (possibly including the rescaling method proposed below), for now we choose the entropy of the background model $S_0 = -\frac{1}{M} \ln \mathcal{P}(\mathbf{X}|0, 0) = -\frac{1}{M} \sum_i \ln \mathcal{P}_i (\mathbf{X}_i^T | 0, 0)$ as reference point, where $\mathcal{P}_i (\mathbf{X}_i^T | 0, 0) = \frac{1}{\mathcal{Z}_0} \mathrm{Tr}' \mathrm{e}^{-\mathcal{H}_0 (\mathbf{X}_i^T)}$ is the probability of a single column under the phylogenetic model equation (3) with $\mathcal{Z}_0 = \mathrm{Tr}\, \mathrm{e}^{-\mathcal{H}_0}$. Integrating a common preprocessing step, the entropy difference of single columns ΔS_i or pairs of columns ΔS_{ij} can then conveniently be used to decide which loci exhibit significant deviations from the background model and should be included in the inference.

1.3.3. Background estimation. $3M - 3$ coefficients $\hat{\mathbf{g}}$ and $\hat{\mathbf{K}}$ of the phylogenetic Hamiltonian $\mathcal{H}_0$ need to be estimated from background data which plausibly evolved undisturbed by any fields $\mathbf{h}$ or couplings $\mathbf{J}$. For instance, in a protein sequence alignment one could take less conserved columns that are usually not used to infer evolutionary correlations. Given N_0 uncorrelated columns of such background data $\mathbf{X}^{(0)}$, one would then match marginal distributions $\pi_\alpha = \frac{1}{2N_0} \sum_i (X_{\alpha i}^{(0)} + 1)$ and $\pi_{\alpha\beta} = \frac{1}{4N_0} \sum_i (X_{\alpha i}^{(0)} + 1)(X_{\beta i}^{(0)} + 1)$ to the theoretical marginals $P_1(x_\alpha = 1)$ and $P_2(x_\alpha = 1, x_\beta = 1) = P_1(x_\alpha = 1 | x_\beta = 1) P_1(x_\beta = 1)$ by nonlinear least squares, using equations (20) and (22) to compute the marginals. Appropriate pseudo-counts or regularization terms should be added when estimating background parameters directly from data to avoid overfitting and reduce noise. Alternatively, if a phylogenetic Markov model for the relevant genomic regions of the species of interest is known, one could use it to calculate the marginals and then fit parameters $\mathbf{g}$ and $\mathbf{K}$. For the phylogenies of figure 3, we used our explicit Ising model on a perfect binary tree from which leaves were sampled, and then fitted the coefficients of $\mathcal{H}_0$ on the induced topology by exactly calculating marginals for corresponding leaves via equation (20).

2. Results

2.1. Analytical results for a simplified correlation structure

To gain insight into the effect of between-sample correlations on inference, we first consider a simplified version of the problem. Instead of a branching process giving rise to a tree structure of between-sample correlations, we assume these correlations have the structure of a linear chain, as would happen if samples were taken from a time series or a Markov chain. We do not attempt to explicitly model the process that gives rise to these correlations, but assume that a linear Ising chain with intra-chain coupling K_0 is a sufficiently accurate description. This coupling could be estimated from background data $X^{(0)}$ for N_0 uncorrelated loci via $\tanh \hat{K} = \frac{1}{MN_0}\sum_{\alpha,i} X_{\alpha i}^{(0)} X_{(\alpha+1)i}^{(0)}$.

In section 1.2.2, we detailed how optimal values $\hat{h}_i$ and $\hat{J}_{ij}$ can be inferred from the observed moments m_i and m_{ij} when treating different sites or site pairs independently:

$$\tanh \hat{h}_i = \frac{\left(1 - \hat{R}\right)m_i}{\sqrt{\left(1 + \hat{R}\right)^2 - 4m_i^2 \hat{R}}}, \tag{24a}$$

$$\tanh \hat{J}_{ij} = \frac{\left(1 - \hat{R}^2\right)m_{ij}}{\sqrt{\left(1 + \hat{R}^2\right)^2 - 4m_{ij}^2 \hat{R}^2}}. \tag{24b}$$

As expected, these estimates depend on the assumed intra-chain coupling $\hat{R} = \tanh \hat{K}$. Ignoring the phylogenetic correlations between samples (by taking $\hat{K} = 0$ and therefore $\hat{R} = 0$) would yield higher $\hat{h}_i$ and $\hat{J}_{ij}$ than when using a finite value.

Due to the coherent fluctuations induced by the between-sample correlations, the sample averages m_i and m_{ij} can be only poor estimators for the ensemble averages required for accurate inference. Above, the leading order contribution to the expected inference errors $\Delta\hat{h}_i^2 = \langle(\hat{h}_i - h_i)^2\rangle$ and $\Delta\hat{J}_{ij}^2 = \langle(\hat{J}_{ij} - J_{ij})^2\rangle$ was calculated as

$$\Delta\hat{h}_i^2 = h_i^2\left(e^{-2(\hat{K}-K_0)} - 1\right)^2 + \frac{e^{-2(2\hat{K}-K_0)}}{M}, \tag{25a}$$

$$\Delta\hat{J}_{ij}^2 = J_{ij}^2\left(\frac{\cosh 2K_0}{\cosh 2\hat{K}} - 1\right)^2 + \frac{\cosh 2K_0}{M\cosh^2 2\hat{K}}. \tag{25b}$$

The first term stems from the error made for the 'average' configuration when neglecting or misestimating $\hat{K} \neq K_0$. It vanishes for perfect knowledge about the intra-chain correlations ($\hat{K} = K_0$), in which case the estimates for the fields **h** and couplings **J** do not incorrectly account for background correlations. The second term is a finite-size error, coming from coherent fluctuations of single finite configurations about the average, and it therefore scales as $1/M$. Indeed, finite-size errors exist even in the uncoupled case **h** = **J** = 0. While the effect of finite size fluctuations can be reduced by overestimating $\hat{K}$, the first term dominates for any sample of reasonable size, and the total error is minimized at (or very near) $\hat{K} = K_0$.
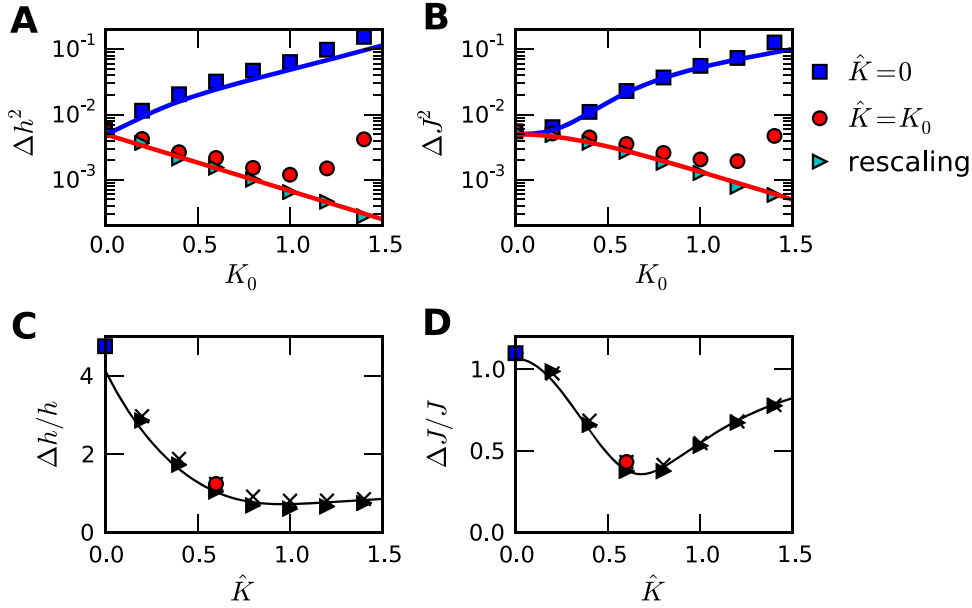
Figure 2. Results for samples on a linear chain. Inference errors in fields (A) and coupling (B) as function of K_0. Errors are exponentially smaller when using the correct estimate $\hat{K} = K_0$ for the coupling between samples. Relative inference errors $\Delta h/h$ (C) and $\Delta J/J$ (D) as function of the assumed intra-chain coupling $\hat{K}$, with $K_0 = 0.6$ fixed (other parameters as in (A) and (B)). For finite M, the optimal $\hat{K}$ is slightly larger than K_0, and rescaling (triangles) gives similar results as exact inference (crosses). Solid lines are from equation (25), with $\Delta h = \sqrt{\Delta h^2}$ and $\Delta J = \sqrt{\Delta J^2}$ in (C) and (D). Error bars from averaging 1000 configurations are smaller than symbol size.

To validate these results, we consider a system with $N = 2$ loci and $M = 200$ samples, varying the impact of correlations between the samples by increasing K_0. At the same time, we use an adjusted coupling $J_{12} = 0.25/\cosh 2K_0$ and fields $h_{1/2} = 0.125\, e^{-2K_0}$ to guarantee that m_1, m_2 and m_{12} are roughly independent of K_0, while the amplitude of coherent fluctuations increases with K_0. To obtain representative configurations of this system we simulated the model using a cluster Monte Carlo algorithm [35, 36]. Then we inferred $\hat{h}_{1/2}$ and $\hat{J}_{12}$ from each configuration (separately) via numerical minimization of the entropy $\mathcal{S}$ as in section 1.2.1. Figure 2 shows the mean squared error in our inference across the sampled configurations as function of K_0 or $\hat{K}$, respectively, and confirms our expectations from equation (25). Discrepancies between theory and numerical results for higher K_0 are mainly due to frozen configurations which are affected by regularization. Note that *relative* inference errors $\Delta\hat{h}/h$ and $\Delta\hat{J}/J$ are dominated by a global trend from our choice of adjusting fields and couplings with K_0, and are therefore less feasible for a comparison of results across K_0-values and between methods.

Intriguingly, to leading order in m_i or m_{ij}, the estimates in equation (24) become independent of $\hat{K}$ if rescaled values $\tilde{m}_i \equiv m_i e^{-2\hat{K}}$ and $\tilde{m}_{ij} \equiv m_{ij}/\cosh 2\hat{K}$ are used. This suggests that we can simply infer $\hat{\mathbf{h}}$ and $\hat{\mathbf{J}}$ from these rescaled moments and otherwise ignore correlations between samples. The triangles in figure 2 validate this procedure for our simulated data. Indeed, it works even slightly better than numerical minimization, mainly because
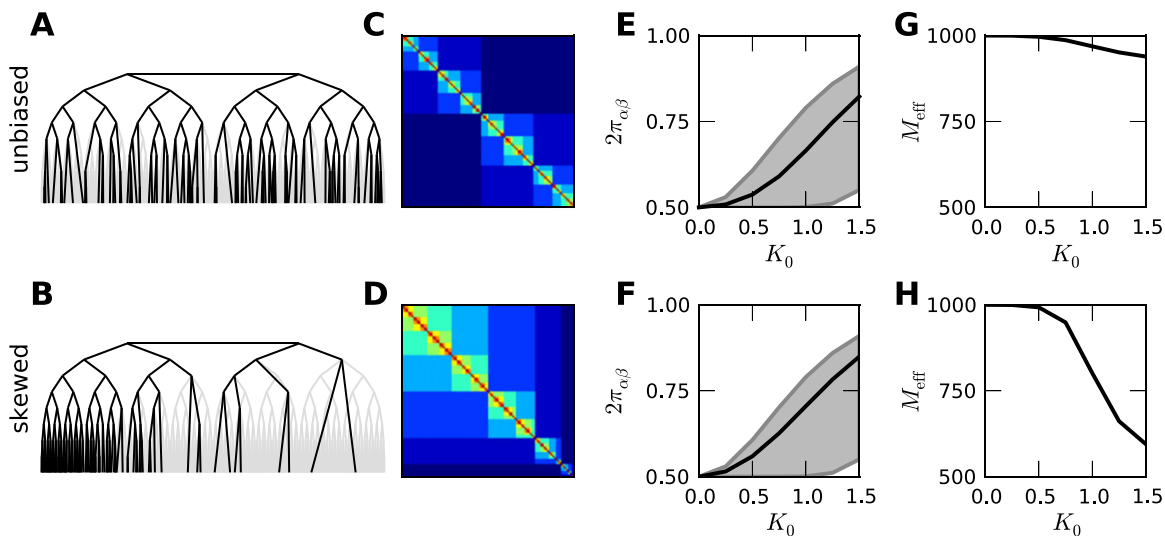
Figure 3. Creating phylogenetic trees. (A), (B) Phylogenies are created by sampling $M = 1000$ leaves from a perfect binary tree of 12 levels (gray; shown here with nine levels and $M = 100$) either in an unbiased (top row) or a skewed way (bottom row) to mimic sampling bias. Parameters for the new topologies (black) are inferred from phylogenetic correlations $\chi_{\alpha\beta}$ (shown as heatmaps (C) and (D)). (E), (F) Range of sequence similarity $2\pi_{\alpha\beta}$ (shaded) and average similarity between most similar sequences (line). (G), (H) Effective number of independent samples calculated from the information context of the weights distribution w_α.

singularities due to frozen configurations are entirely avoided, and it is also useful when $\hat{K}$ is not precisely estimated.

2.2. Numerical approach for correlations with a tree structure

We now turn to the biologically motivated problem where the interactions between species follow a tree structure. In contrast to the above first-order analysis, we aim to infer all fields **h** and couplings **J** simultaneously. Our approach is based on maximizing the likelihood of the model parameters **h** and **J** using equation (2), with the Hamiltonian equation (3). Parameters $\hat{g}_\alpha$ and $\hat{K}_{\alpha\beta}$ of the phylogenetic background model $\mathcal{H}_0$ (equation (4)) are assumed to be known; they can be separately inferred from appropriate background data (see section 1.3.3). As detailed in section 1.3, we can in principle evaluate equation (2) by condensing all N values $\mathbf{X}_\alpha$ from one species (i.e., one row in figure 1) into a single 2^N-state Potts variable. The interaction graph between these variables has a tree topology, and the partition function can be evaluated in a time linear in M using belief propagation [20]. The computational cost of this procedure grows as $M2^{2n}$, which is obviously infeasible for systems with more than a handful of loci (i.e., larger N). As a solution, we combine this approach with an adaptive cluster expansion method [21, 22], in order to decompose the system into a collection of clusters of manageably small size, comprising only strongly interacting members. Fields and couplings are then inferred for each cluster separately. Briefly, the procedure starts from pairs of loci and tests for correlations by comparing the entropy (or log-likelihood) of models with and without an interaction term.
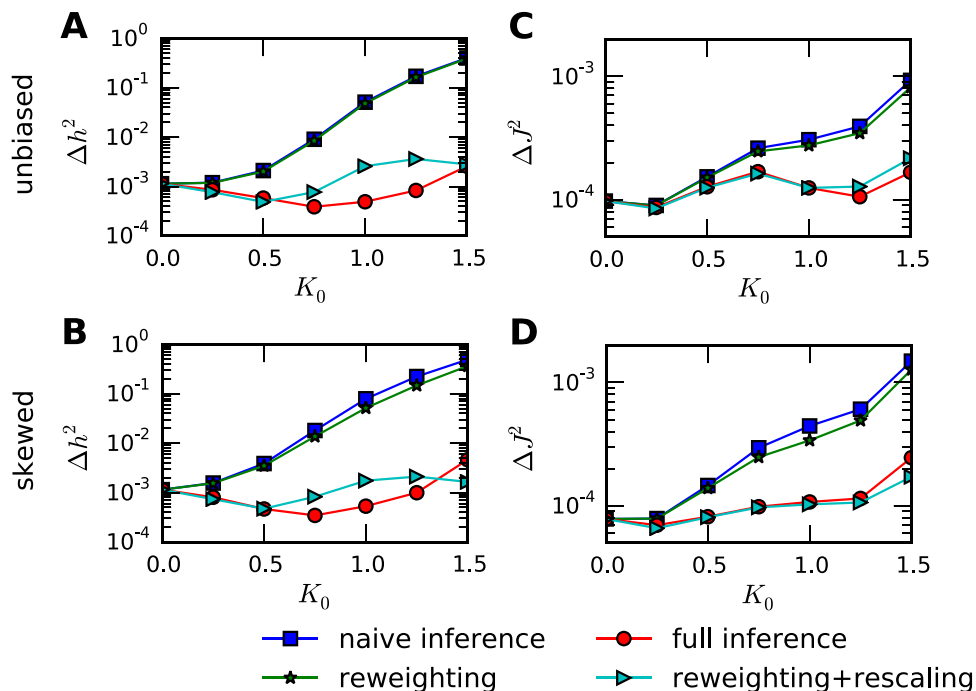
Figure 4. Results for samples on a tree. Errors in reconstructed fields Δh^2 (A), (B) and couplings ΔJ^2 (C), (D) for a system of $N = 20$ loci for different inference methods as indicated. The interaction matrix **J** is sparse with N entries $J_{ij} = \pm 0.25/\cosh 2K_0$ such that no more than 3 loci are connected, and fields are uniform random numbers $|h_i| \leqslant 0.125\,\mathrm{e}^{-2K_0}$. For a tree structure this adjustment with K_0 does not keep the values m_i and m_{ij} entirely constant, but it helps to avoid frozen configurations. Error bars from averaging over ten configurations each for ten different instances of **h** and **J** are smaller than symbol size.

This interaction is included, and the procedure is iterated to possibly expand the cluster, only if it brings a significant improvement in likelihood beyond a predefined threshold.

Tree generation.   For the case of phylogenetic correlations we aim to emulate a biological problem. We create a plausible tree topology by sampling M leaves from an initial perfect binary tree with homogeneous neighbor couplings $K_{\alpha\beta} \equiv K_0$ (figure 3(A), (B)). The phylogenetic correlations between the chosen leaves are used to numerically infer the non-homogeneous parameters of the Hamiltonian $\mathcal{H}_0$ on the induced phylogeny just as would be done with real data. In terms of observables relevant in a biological context, the phylogenetic correlations are indicative of the sequence identity between two samples (the fraction of identical spins). For *a priori* equiprobable binary states (i.e., $g_\alpha \equiv 0$), this is calculated from $2\pi_{\alpha\beta} = \frac{1}{2}(\mu_{\alpha\beta} + 1)$, which ranges from 0.5 for perfectly uncorrelated samples to 1 for perfectly correlated ones. Note that for all values $K_0 \lesssim 1$ some of the samples are actually entirely uncorrelated (see figure 3(E), (F)). Mimicking frequently observed sampling bias leading to a more heterogeneous correlation structure, we also create 'skewed' topologies, where we preferentially sample leaves from one side of the tree (second row in figure 3).
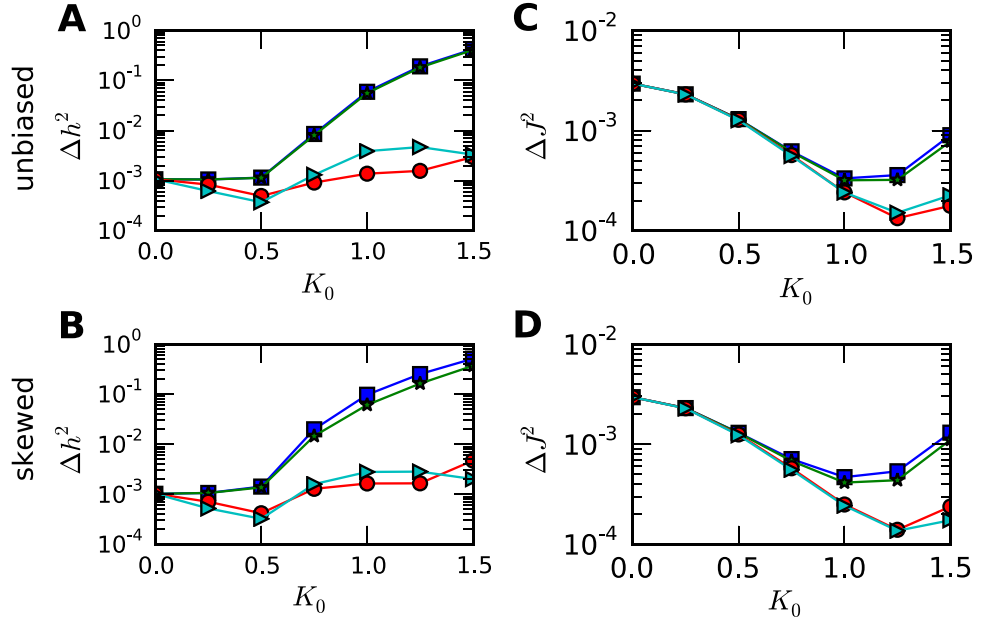
Figure 5. As in figure 4 for $N = 20$, but for a Sherrington–Kirkpatrick spin glass with $h_i \equiv 0$ and J_{ij} drawn from a Gaussian distribution with standard deviation $0.25/\cosh 2K_0/\sqrt{N}$.

Simulation results. Choosing **h** and **J** as described in the legend of figures 4 and 5, we generate configurations $\mathbf{X}'$ for N loci on the induced phylogeny by Monte Carlo sampling [35, 36]. These simulated configurations are used next to reconstruct values $\hat{\mathbf{h}}$ and $\hat{\mathbf{J}}$, respectively. For a relatively simple inference problem with sparse matrix **J**, figure 4 shows the resulting mean squared errors $\Delta h^2 = \frac{1}{N}\sum_i \langle (\hat{h}_i - h_i)^2 \rangle$ and $\Delta J^2 = \frac{2}{N(N-1)}\sum_{i<j} \langle (\hat{J}_{ij} - J_{ij})^2 \rangle$, as a function of the phylogenetic coupling strength K_0 on the initial tree from which the leaves were sampled. We compare our method ('full inference') with a 'naive' averaging using $\mathcal{H}_0 = 0$, where the entropy is given by the familiar expression

$$S_{\text{uc}} = \frac{1}{M}\ln\mathcal{Z}_{\text{uc}} - \sum_i h_i m_i - \sum_{i<j} J_{ij} m_{ij}. \tag{26}$$

Here, $\mathcal{Z}_{\text{uc}}$ is the partition sum for the Hamiltonian equation (3) for uncorrelated samples ($\mathcal{H}_0 = 0$) and the averages m_i and m_{ij} are obtained as before by averaging over the columns of **X**.

Figure 4 demonstrates that the reconstruction errors are systematically and significantly smaller using the full inference. For better comparison between methods, we select clusters always based on differential cluster entropies for the full inference. We used a cluster threshold $\Theta = e^{-K_0}/M$ chosen after inspection of pair entropies ΔS_{ij}. Otherwise, a method that is unaware of the phylogeny will always yield more clusters due to larger log-likelihood differences ΔS, because deviations that are actually due to phylogenetic correlations are 'explained' by larger values for the fit parameters **h** and **J**. Similar results are obtained for a different inference problem (the Sherrington–Kirkpatrick spin glass, figure 5). Since the trends of figure 2 carry over to the specific correlation structure associated with phylogenies, our analytical results are useful to understand the global inference problem.
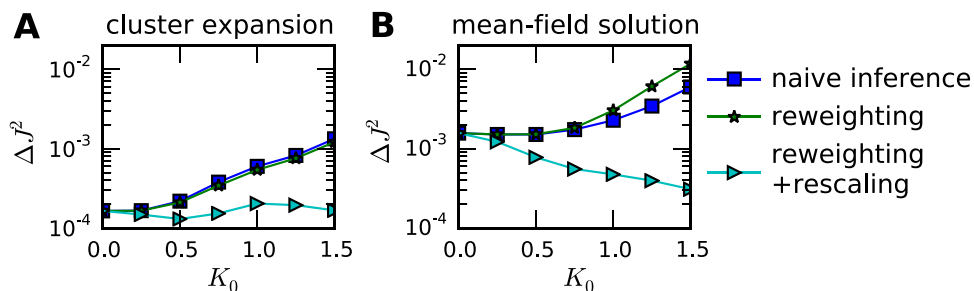
Figure 6. Results for a larger system with $N = 50$ nodes and $M = 1000$ samples from the skewed phylogeny of figure 4. Here, $J_{ij} = \pm 0.25/\cosh 2K_0$ has $2N$ non-zero entries in clusters of up to 10 connected loci, and fields are as in figure 4. Errors in reconstructed couplings are shown for the cluster expansion (A) or the mean-field approach (B).

Rescaling versus reweighting. Previous work often used a simple reweighting approach to account for phylogenetic correlations, based on a differential weighting of samples when calculating moments from empirical observations, such that $\tilde{m}_i = \sum_\alpha w_\alpha X_{\alpha i}$ and $\tilde{m}_{ij} = \sum_\alpha w_\alpha X_{\alpha i} X_{\alpha j}$. For comparing to reweighting schemes, we focused on one method suitable in our context. Here, the weights $w_\alpha = \sum_\beta \chi_{\alpha\beta}^{-1} / \sum_{\gamma\delta} \chi_{\gamma\delta}^{-1}$ are calculated from the inverse of the phylogenetic correlation matrix $\chi_{\alpha\beta} = \frac{1}{4}(\mu_{\alpha\beta} - \mu_\alpha \mu_\beta)$. This gives the maximum likelihood estimate for the mean of a sample drawn from a multivariate Gaussian distribution [26]. The loss of information associated with reweighting can easily be quantified by calculating the information content $I(w) = -\sum_\alpha w_\alpha \ln w_\alpha$ of the weights distribution, and a resulting effective number of independent sequences $M_{\text{eff}} = e^{I(w)}$. This reweighting scheme captures the heterogeneous structure of the phylogenetic correlations and accounts for the redundancy in the data (figure 3(G), (H)).

Results for 'naive' inference with reweighting are presented as stars in figures 4 and 5, and indicate significant but comparatively minor improvements, especially for the inferred couplings $\hat{\mathbf{J}}$ (see also [9]). This implies that the specific structure of the phylogenetic tree is much less important than the overall sequence similarity in the sample. The correspondence between figures 2 and 4 therefore suggests to augment the reweighting method with a heuristic rescaling scheme, $\tilde{m}_i \to \tilde{m}_i e^{-2K_{\text{eff}}}$ and $\tilde{m}_{ij} \to \tilde{m}_{ij}/\cosh 2K_{\text{eff}}$ for $i \neq j$. The effective coupling K_{eff} serves to connect correlations on the phylogenetic tree to correlations of a linear chain. We use a well-known result for the spin–spin correlation function on a tree [37] to calculate an estimate $\tanh^2 K_{\text{eff}} = \frac{2}{M} \sum_\alpha \max_{\beta \neq \alpha} 2\pi_{\alpha\beta} - 1$ from the average sequence similarity between most similar sequence pairs (see figure 3(E), (F)). As shown by the triangles in figures 4 and 5, this simple method of globally removing phylogenetic bias significantly decreases the inference error down to the level of the full inference, even for correlations with an underlying tree structure.

3. Discussion

3.1. The mean-field solution

Recent biological applications relied on a simple mean-field approach [8–11], where the couplings are inferred by inverting the matrix $C_{ij} = m_{ij} - m_i m_j$ of connected correlations:

$$\hat{J}_{ij} = -\left(C^{-1}\right)_{ij}. \tag{27}$$

To test the performance of this method in the presence of phylogenetic correlations and to compare to reweighting and rescaling schemes, we simulated data with the same phylogenies as before, but a larger system of $N = 50$ loci. Figure 6 shows results of the inference using the cluster expansion or the mean-field method (with a pseudocount to handle insufficient variability), respectively. We did not include the full inference, since for larger systems with clusters of size n the time complexity scales as $M2^{2n}$ and additionally suffers from roundoff errors in the message passing recursions, leading to slow convergence of the minimization routines. Without the full inference as standard, we decided to include clusters based on the naive method, with the cluster threshold $\Theta = .1/M$ held fixed. Generally, the mean-field solution is less accurate than the cluster expansion, but these alternative methods follow similar trends: rescaling is very effective in removing phylogenetic biases, while reweighting is only marginally beneficial (due to a different quantitative effect of the pseudocount it actually performs worse than the naive method for larger K_0).

3.2. Connection to standard phylogenetic models

Phylogenetic inference is usually performed using Markov models. For binary data, such models require $2M - 3$ parameters (the length of each branch on the associated tree) plus one value setting the equilibrium frequency (the relative proportion of the two values). These values are fit to data using recursive algorithms largely equivalent to the ones used here [38]. The commonly used substitution matrices also imply reversibility of the underlying stochastic process, and the assumption that the equilibrium frequency does not change along the tree. However, a simple interpretation of their parameters (e.g., branch lengths as expected substitutions per time) warrants some caution, since substitutions are not the only cause of sequence change and their rates or the relevant time unit not necessarily constant along the tree, and because other assumptions about homology and evolutionary processes enter the preparation of the alignment in the first place. More cautiously, these models can be seen as optimal descriptions of the available data within the considered space of models.

Hence we argue that our choice for describing phylogenetic correlations by means of a phylogenetic Hamiltonian is not a limiting factor, because it is merely a generalization of a Markov model to a Markov random field, allowing for different equilibrium frequencies on different leaves [39]. Alternatively, our entire approach could easily be reformulated in the language of phylogenetic models [40], leading to similar recursions [38]. In any case, apart from conceptual clarity and straightforward techniques for generating simulation data, we believe that our non-standard formalism is advantageous under circumstances where the data are poorly fit by an explicit phylogenetic model. This could be the case due to non-uniform sequencing quality or alignability between samples, leading to an uneven distribution of gaps in the alignment. Gaps are often included as additional states, but standard Markov models prescribe constant gap frequencies along the tree [41] whereas we can use different priors for each species. Further, our approach could be favorable if the data represent states of larger genomic regions, such as cis-regulatory elements, whose evolution is best described on a more coarse-grained scale. We note that exploiting the correspondence between evolutionary dynamics and Ising models has a long tradition [31]. A similar phylogenetic Ising model has recently been used to model HIV sequence statistics [42].

3.3. Inference on protein alignments

Inverse Ising inference has found a powerful application in the prediction of residue contacts from large protein alignments (where it is often called direct coupling analysis [8–11, 25]). These analyses use sequences from large protein families spanning considerable evolutionary distances, such that neutral positions in the alignment can generally be considered as independent. Still, there are typically subsets of sequences from more closely related species where this assumption is violated. In principle, our method can be readily adapted to non-binary data, corresponding to formulating the Hamiltonian equation (3) in terms of Potts variables with $\Lambda = 21$ states (for 20 amino acids and a gap). In this case, we anticipate that it might be difficult to reliably estimate all associated parameters. Also, the complexity of the cluster expansion method combined with the message passing grows like $M\Lambda^{2n}$ for a cluster of n columns, which would quickly become prohibitive. Further, published methods for genomics-aided protein structure prediction [8–11] only require the identification of a small number of putative residue contacts from the top interacting pairs, and the pair ranking has been observed to be quite robust with regard to phylogenetic reweighting [5, 9]. However, for more quantitative applications (see, e.g., [7, 12]), we propose the mean-field approach combined with our rescaling method as simple yet effective strategy. This mainly involves shifting measured sample averages closer to the background distribution because deviations are partially attributed to coherent fluctuations. It ameliorates problems with the proper choice of regularizers, and only requires knowledge of this background distribution and of the average sequence identity in the sample. Both can usually be reliably estimated in current sequence data sets.

4. Conclusions

We presented a systematic study of inverse Ising inference for phylogenetically correlated samples, based on combining belief propagation recursions with an adaptive cluster expansion method proposed previously [21]. Here, we employed an Ising-like background model that generates the observed phylogenetic correlations. We then maximize the likelihood of interaction coefficients between different loci in adaptively chosen small clusters, given the corresponding data and the background model. Our method significantly reduces the inference error due to phylogenetic bias. Our focus here was on phylogenetic correlations between samples, but we note that such correlation may arise from slow dynamical processes in other contexts unrelated to biology. Finally, we emphasize that there might also be circumstances where biases due to phylogeny or other processes can safely be neglected, for instance if only the interaction topology (i.e., non-zero entries of $\hat{\mathbf{J}}$ regardless of their exact value) is of interest [24, 33, 34], but this question warrants further research.

Popular approaches for mitigating the effect of phylogenetic bias are based on down-weighting highly similar samples, but we show here that this has only marginal benefits. In contrast, we propose a simple rescaling of observed averages by the expected contribution attributed to excess sequence similarity, and show that it can be highly effective. Importantly, this undemanding approach is very useful even when the inference is based on simple (and computationally inexpensive) mean-field inference, which is now frequently used in the field of protein folding.

Acknowledgments

References

[1] Schneidman E, Berry M J, Segev R and Bialek W 2006 Weak pairwise correlations imply strongly correlated network states in a neural population *Nature* **440** 1007–12

[2] Bialek W, Cavagna A, Giardina I, Mora T, Silvestri E, Viale M and Walczak A M 2012 Statistical mechanics for natural flocks of birds *Proc. Natl Acad. Sci. USA* **109** 4786–91

[3] Lee E D, Broedersz C P and Bialek W 2013 Statistical mechanics of the US supreme court (arXiv:1306.5004)

[4] Lezon T R, Banavar J R, Cieplak M, Maritan A and Fedoroff N V 2006 Using the principle of entropy maximization to infer genetic interaction networks from gene expression patterns *Proc. Natl Acad. Sci. USA* **103** 19033–8

[5] Weigt M, White R, Szurmant H, Hoch J and Hwa T 2008 Identification of direct residue contacts in protein–protein interaction by message passing *Proc. Natl Acad. Sci. USA* **106** 67–72

[6] Santolini M, Mora T and Hakim V 2013 Beyond position weight matrices: nucleotide correlations in transcription factor binding sites and their description (arXiv:1302.4424)

[7] Mann J K, Barton J P, Ferguson A L, Omarjee S, Walker B D, Chakraborty A and Ndungú T 2014 The fitness landscape of HIV-1 gag: advanced modeling approaches and validation of model predictions by *in vitro* testing *PLoS Comput. Biol.* **10** e1003776

[8] Marks D S, Colwell L J, Sheridan R, Hopf T A, Pagnani A, Zecchina R and Sander C 2011 Protein 3D structure computed from evolutionary sequence variation *PLoS One* **6** e28766

[9] Morcos F, Pagnani A, Marks D S, Sander C, Zecchina R, Onuchic J N, Hwa T and Weigt M 2011 Direct-coupling analysis of residue coevolution captures native contacts across many protein families *Proc. Natl Acad. Sci. USA* **108** 1293–301

[10] Hopf T A, Colwell L J, Sheridan R, Rost B, Sander C and Marks D S 2012 Three-dimensional structures of membrane proteins from genomic sequencing *Cell* **149** 1607–21

[11] Sulkowska J I, Morcos F, Weigt M, Hwa T and Onuchic J N 2012 Genomics-aided structure prediction *Proc. Natl Acad. Sci. USA* **109** 10340–5

[12] Morcos F, Schafer N P, Cheng R R, Onuchic J N and Wolynes P G 2014 Coevolutionary information, protein folding landscapes, and the thermodynamics of natural selection *Proc. Natl Acad. Sci.* **111** 12408–13

[13] Jaynes E 1957 Information theory and statistical mechanics *Phys. Rev. E* **106** 620–30

[14] Jaynes E 1957 Information theory and statistical mechanics: II. *Phys. Rev. E* **108** 171–90

[15] Lapedes A S, Giraud B, Liu L and Stormo G D 1999 Correlated mutations in models of protein sequences: phylogenetic and structural effects *Institute of Mathematical Statistics* (Hayward, CA) pp 236–56 (projecteuclid.org)

[16] Sessak V and Monasson R 2009 Small-correlation expansions for the inverse Ising problem *J. Phys. A: Math. Theor.* **42** 055001

[17] Kappen H J and Rodriguez F B 1998 Efficient learning in boltzmann machines using linear response theory *Neural Comput.* **10** 1137–56

[18] Tanaka T 1998 Mean-field theory of Boltzmann machine learning *Phys. Rev. E* **58** 2302

[19] Nguyen H and Berg J 2012 Mean-Field theory for the inverse ising problem at low temperatures *Phys. Rev. Lett.* **109** 050602

[20] Mezard M and Montanari A 2009 *Information, Physics and Computation* (Oxford: Oxford University Press)

[21] Cocco S and Monasson R 2011 Adaptive cluster expansion for inferring Boltzmann machines with noisy data *Phys. Rev. Lett.* **106** 090601

[22] Cocco S and Monasson R 2012 Adaptive cluster expansion for the inverse Ising problem: convergence, algorithm and tests *J. Stat. Phys.* **147** 252–314

[23] Ravikumar P, Wainwright M J and Lafferty J D 2010 High-dimensional Ising model selection using l(1)-regularized logistic regression *Ann. Stat.* **38** 1287–319

[24] Aurell E and Ekeberg M 2012 Inverse Ising inference using all the data *Phys. Rev. Lett.* **108** 090201

[25] Cocco S, Monasson R and Weigt M 2013 From principal component to direct coupling analysis of coevolution in proteins: low-eigenvalue modes are needed for structure prediction *PLoS Comput. Biol.* **9** e1003176

[26] Altschul S F, Carroll R J and Lipman D J 1989 Weights for data related by a tree *J. Mol. Biol.* **207** 647–53

[27] Gerstein M, Sonnhammer E L and Chothia C 1994 Volume changes in protein evolution *J. Mol. Biol.* **236** 1067–78

[28] Plerou V, Gopikrishnan P, Rosenow B, Amaral L A N, Guhr T and Stanley H E 2002 Random matrix approach to cross correlations in financial data *Phys. Rev.* E **65** 066126

[29] Halabi N, Rivoire O, Leibler S and Ranganathan R 2009 Protein sectors: evolutionary units of three-dimensional structure *Cell* **138** 774–86

[30] Dutheil J Y 2012 Detecting coevolving positions in a molecule: why and how to account for phylogeny *Brief. Bioinform.* **13** 228–43

[31] Leuthäusser I 1986 An exact correspondence between eigen evolution model and a two-dimensional Ising system *J. Chem. Phys.* **84** 1884–5

[32] Nocedal J and Wright S J 2006 *Numerical Optimization* (New York: Springer)

[33] Donoho D L and Elad M 2003 Optimally sparse representation in general (nonorthogonal) dictionaries via ℓ^1 minimization *Proc. Natl Acad. Sci. USA* **100** 2197–202

[34] Andrew G and Gao J 2007 Scalable training of L_1-regularized log-linear models *Proc. 24th Int. Conf. on Machine Learning* (ACM: New York) pp 33–40

[35] Wolff U 1989 Collective Monte Carlo updating for spin systems *Phys. Rev. Lett.* **62** 361

[36] Newman M E J and Barkema G T 1996 Monte carlo study of the random-field Ising model *Phys. Rev.* E **53** 393–404

[37] Mukamel D 1974 2-Spin correlation-function of spin 1/2 Ising-model on a Bethe lattice *Phys. Lett.* A **50A** 339–40

[38] Felsenstein J 1981 Evolutionary trees from DNA sequences: a maximum likelihood approach *J. Mol. Evol.* **17** 368–76

[39] Wainwright M J and Jordan M I 2007 Graphical models, exponential families, and variational inference *Found. Trends Mach. Learn.* **1** 1–305

[40] Siepel A and Haussler D 2004 Phylogenetic estimation of context-dependent substitution rates by maximum likelihood *Mol. Biol. Evol.* **21** 468–88

[41] Rivas E and Eddy S R 2008 Probabilistic phylogenetic inference with insertions and deletions *PLoS Comput. Biol.* **4** e1000172

[42] Shekhar K, Ruberman C F, Ferguson A L, Barton J P, Kardar M and Chakraborty A K 2013 Spin models inferred from patient-derived viral sequence data faithfully describe HIV fitness landscapes *Phys. Rev.* E **88** 062705